Compensator Design for Closed Loop Hall-Effect Current Sensors

Ashish Kumar and Vinod John
Department of Electrical Engineering, Indian Institute of Science, Bangalore - 560012, India.
Email: ashishk@ee.iisc.ernet.in, vjohn@ee.iisc.ernet.in

***Abstract*—Closed loop current sensors used in power electronics applications are expected to have high bandwidth and minimal measurement transients. In this paper, a closed loop compensated Hall-effect current sensor is modeled. The model is used to tune the sensor's compensator. Analytical expression of step response is used to evaluate the performance of the PI compensator in the current sensor. This analysis is used to devise a procedure to design parameters of the PI compensator for fast dynamic response and for small dynamic error. A prototype current sensor is built in the laboratory. Simulations using the model are compared with experimental results to validate the model and to study the variation in performance with compensator parameters. The performance of the designed PI compensator for the sensor is compared with a commercial current sensor. The measured bandwidth of the designed current sensor is above 200 kHz, which is comparable to commercial standards. Implementation issues of PI compensator using operational amplifiers are also addressed.**

***Index Terms*—Closed loop current sensors, Hall sensor, current probe, current sensor model, sensor compensation**

SYMBOLS AND ABBREVIATIONS

i_1	: Primary current, current to be measured
i_2	: Secondary current, compensating current
n_1	: Number of primary turns
n_2	: Number of secondary turns
ϕ_c	: Magnetic flux in the core
λ_2	: Flux linked with secondary coil
B_g	: Magnetic flux density in air gap
H_g	: Magnetic field intensity in air gap
l_g	: Air gap length
H_m	: Magnetic field intensity in the core
l_m	: Mean length of the core
A_c	: Cross-sectional area of the core
μ_r	: Relative permeability of the core
r_2	: Winding resistance of secondary coil
R_B	: Burden resistance
v_H	: Hall element output voltage
K_h	: Sensitivity of Hall element
B_H	: Perpendicular component of the magnetic field over the Hall element
$G_c(s)$	: Compensator transfer function
V_{out}	: Voltage drop across the burden resistor

I. INTRODUCTION

Current sensors are widely used in power electronics systems including switched mode power converters, electric machine drives, grid connected power converters, etc. A number of these applications require current measurement with galvanic isolation. Current transformers cannot measure direct currents and have large error at low frequency currents. A modified CT structure using Hall element, also known as Hall-effect current sensor is commonly used in isolated current measurement applications. Analysis of closed loop compensated Hall-effect current sensors was reported in [1]- [4]. In [3] it was shown that high gain of proportional compensator results in significant improvement in steady state performance of these sensors. High frequency model employing control component and system identification presented in [4] further helped in analysis upto MHz range. However, modeling of the current sensor with the objective of designing its compensator parameters is not available.

In this paper operational principles of closed loop compensated Hall-effect current sensor is discussed briefly. An equivalent circuit is derived using some practical assumptions, which facilitates the analysis of these sensors. Closed form analytical expressions of step response are derived for the current sensor with a PI compensator. This is used to show the effect of changing the control parameters on the dynamic performance. Based on these expressions a procedure is devised to tune the parameters of PI compensator for high precision current measurement. This study involves analysis to develop high performance AC/DC current sensor comparable to commercially available current sensors [8]. A prototype current sensor is built in laboratory and tested to validate the analysis.

II. MODELING OF CLOSED LOOP COMPENSATED HALL-EFFECT CURRENT SENSOR

A closed loop compensated Hall-effect current sensor is shown in Fig. 1. A Hall element is inserted in the air gap. A conductor carrying current i_1 creates magnetic flux in the core and the air gap. The Hall element produces voltage v_H in response to the air gap magnetic field, which is further amplified by the compensator $G_c(s)$ in order to produce counter magnetic flux in the core due to compensating coil current i_2. This ensures that excitation of the magnetic core is small and lies in linear region of the B-H curve of the core material.

To model the current sensor the following assumptions are made:

- Relative permeability of the magnetic core is very high.

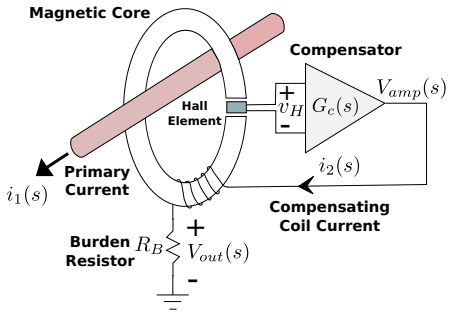

Fig. 1: Closed loop compensated Hall-effect current sensor.

- Leakage inductance and inter-winding capacitance of the compensating winding are ignored.
- Position of the conductor with respect to central axis of the core does not affect the magnetic flux distribution.
- Presence of the Hall element in the air gap does not disturb the field distribution in the air gap.
- Fringing effect in the air gap is ignored.

Derivation of Equivalent Circuit Diagram

Applying Ampere's circuital law, and ignoring reluctance offered by the magnetic core we get

$$n_1 i_1 - n_2 i_2 = H_m l_m + H_g l_g \approx H_g l_g \tag{1}$$

Ignoring fringing in air gap, the core flux can be expressed as:

$$\phi_c = B_g A_c = \frac{\mu_0 A_c n_2}{l_g}\left(\frac{n_1}{n_2} i_1 - i_2\right) = \frac{L_m}{n_2} i_m \tag{2}$$

where

$$i_m = \left(\frac{n_1}{n_2} i_1 - i_2\right), \text{ and } \quad L_m = \left(\frac{n_2^2 \mu_0 A_c}{l_g}\right) \tag{3}$$

i_m is magnetizing current, and L_m is magnetizing inductance, both referred to secondary side. The voltage induced in secondary winding can be written as:

$$\begin{aligned} V_2 &= \frac{d}{dt}\lambda_2 = \frac{d}{dt}(n_2 \phi_c) = \frac{d}{dt}(L_m i_m) \\ &= L_m \frac{d}{dt} i_m \end{aligned} \tag{4}$$

As per configuration of the current sensor set-up shown in Fig. 1,

$$V_{amp}(t) + V_2(t) = (r_2 + R_B) i_2(t) \tag{5}$$

$$V_{amp}(s) = G_c(s) v_H(s) \tag{6}$$

Based on (2)-(5) the equivalent circuit of the current sensor can be represented as shown in Fig. 2(a).

Output voltage of the Hall element, v_H, is given by:

$$v_H = K_h B_H = K_h B_g = K_h \frac{\phi_c}{A_c} \tag{7}$$

Using (2), v_H can be expressed as:

$$v_H = K_h \frac{L_m}{n_2 A_c} i_m \tag{8}$$

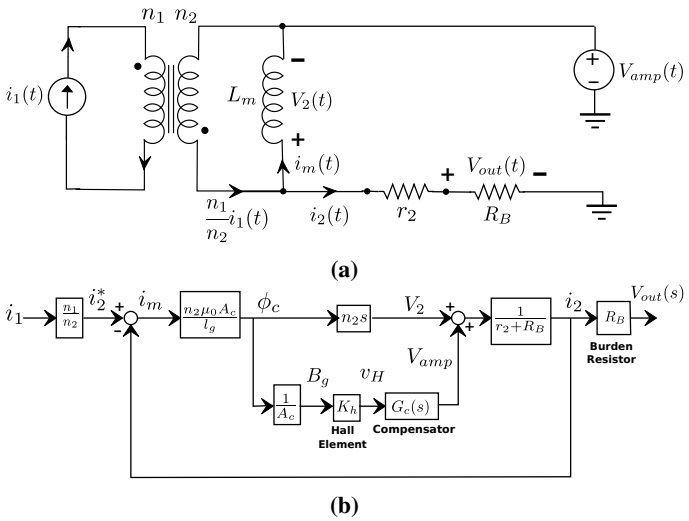

Fig. 2: Models for the closed loop compensated Hall-effect current sensor (a) equivalent circuit model (b) block diagram model.

v_H is the feedback signal corresponding to i_m. It passes through the compensator, $G_c(s)$ to change $V_{amp}(s)$, and in turn, reduces ϕ_c. Using (6), (7) the equivalent circuit can be represented in $s-$domain as a block diagram in Fig. 2(b).

For accurate measurement of i_1 the secondary current i_2 should be ideally equal to $\frac{n_1}{n_2} i_1$. In other words, the magnetizing current, i_m, and hence the core flux ϕ_c, should be brought down close to zero. Using block diagram in Fig. 2(b),

$$\frac{i_2(s)}{i_1(s)} = \frac{n_1}{n_2}\left(\frac{H(s)}{1 + H(s)}\right) \tag{9}$$

and the measurement error function is given by

$$\frac{i_m(s)}{i_1(s)} = \frac{n_1}{n_2}\left(\frac{1}{1 + H(s)}\right) \tag{10}$$

where

$$\begin{aligned} H(s) &= \frac{1}{r_2 + R_B}\left(\frac{n_2^2 \mu_0 A_c}{l_g} s + \frac{n_2 \mu_0 K_h}{l_g} G_c(s)\right) \\ &= \frac{L_m}{r_2 + R_B}\left(s + \frac{K_h}{n_2 A_c} G_c(s)\right) \\ &= \frac{L_m}{R_L}(s + K_m G_c(s)) \end{aligned} \tag{11}$$

and

$$r_2 + R_B = R_L, \qquad \frac{K_h}{n_2 A_c} = K_m \tag{12}$$

Based on (10), to bring i_m close to zero, $H(s)$ must be large over the whole frequency range. $H(s)$ can be further split into two parts as:

$$\begin{aligned} H(s) &= \frac{L_m}{R_L} s + \frac{L_m K_m}{R_L} G_c(s) \\ &= H_{CT}(s) + H_{HE}(s) \end{aligned} \tag{13}$$

In (13) $H_{CT}(s)$ reflects current transformer action, while $H_{HE}(s)$ accounts for the compensation provided by the Hall element. At low frequencies $\|H_{CT}(j\omega)\|$ is very small. Without $H_{HE}(s)$ the magnitude of $H(s)$ also becomes small. Due to the same reason current transformers cannot be used to measure direct and low frequency currents. The compensation $H_{HE}(s)$ is chosen such that its magnitude is large at low frequencies, which can be done by proper selection of $G_c(s)$.

III. Design of the compensator $G_c(s)$

Proportional compensator always results in steady state error in sensor output for DC measurement [3]. The compensator $G_c(s)$ is chosen as proportional-integrator (PI) to eliminate the steady state sensor error. The implementation of $G_c(s)$ as PI compensator is analyzed below:

PI Compensator Design

Using $G_c(s) = K_p + \dfrac{K_i}{s}$ in (11) we get,

$$H(s) = \frac{L_m}{R_L}\frac{(s^2 + K_m K_p s + K_m K_i)}{s} \tag{14}$$

$$= \frac{L_m}{R_L}\frac{(s^2 + 2\zeta_H \omega_n s + \omega_n^2)}{s} \tag{15}$$

where

$$\zeta_H = \frac{K_m K_p}{2\omega_n} \tag{16}$$

$$\omega_n = \sqrt{K_m K_i} \tag{17}$$

The compensator parameters K_p and K_i can be decided, if ζ_H and ω_n are known. These values are chosen based on magnitude frequency response of $H(s)$ in conjunction with step response of the compensated system. As discussed earlier $||H(j\omega)||$ should be kept high throughout the frequency range of interest to minimize error in alternating current measurement.

For a step jump in $i_i(t)$ at $t = 0$ with zero initial condition, $i_1(s) = \frac{I_1}{s}$. Using (9),(14) we get,

$$i_2(s) = \frac{n_1 I_1}{n_2 s}\left(\frac{s^2 + K_m K_p s + K_m K_i}{s^2 + (K_m K_p + \frac{R_L}{L_m})s + K_m K_i}\right) \tag{18}$$

$$= \frac{n_1}{n_2} I_1 \left(\frac{1}{s} - \frac{\frac{R_L}{L_m}}{s^2 + 2\zeta_n \omega_n s + \omega_n^2}\right) \tag{19}$$

where

$$\zeta_n = \frac{K_m K_p + \frac{R_L}{L_m}}{2\omega_n} \tag{20}$$

and ω_n is given by (17).

The second term in (19) represents the fractional error in $i_2(s)$. Based on the damping factor ζ_n the step response may become under damped ($\zeta_n < 1$), critically damped ($\zeta_n = 1$) or over damped ($\zeta_n > 1$). Fig. 3 shows the step response in these conditions for a fixed value of the natural frequency ω_n.

To avoid large peak undershoot in $i_2(t)$ we can select $\zeta_n \geq 1$, but this would increase the settling time. A high value of ζ_n requires high K_p as expressed in (20). Implementation of PI compensator using operational amplifiers puts limitation on maximum value of K_p. Choosing $\zeta_n = 1$ avoids that complexity and provides lower settling time. Using $\zeta_n = 1$ in (19) we get

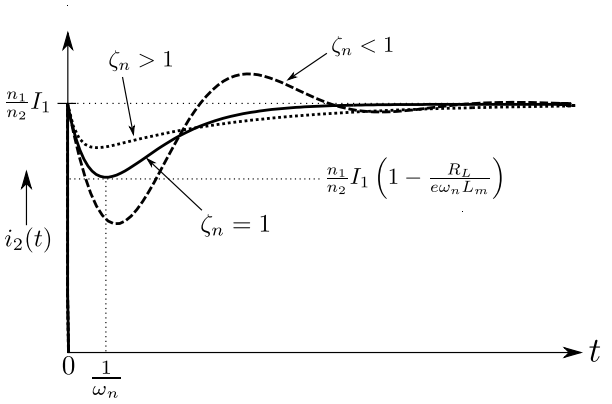

Fig. 3: Step response: $i_2(t)$ for a fixed ω_n and different values of ζ_n.

$$i_2(s) = \frac{n_1}{n_2} I_1 \left(\frac{1}{s} - \frac{\frac{R_L}{L_m}}{(s + \omega_n)^2}\right) \tag{21}$$

Inverse Laplace transform of (21) gives

$$i_2(t) = \frac{n_1}{n_2} I_1 \left(1 - \frac{R_L}{L_m} t e^{-\omega_n t}\right) \tag{22}$$

$i_2(t)$ has minimum value, $I_{2_{min}}$ at $t = t_{min}$, where

$$t_{min} = \frac{1}{\omega_n} \tag{23}$$

$$I_{2_{min}} = \frac{n_1}{n_2} I_1 \left(1 - \frac{R_L}{e\omega_n L_m}\right) \tag{24}$$

In (24) e is the base of natural logarithm. Plot of $i_2(t)$ in (22) is shown in Fig. 3. It is evident from (22) that the steady state error is always zero for DC measurement.

Very low values of t_{min} and the error in $i_2(t)$ are desired for fast dynamics response. It can be achieved with large value of ω_n as shown in (23) and (24). Fig. 4(a) shows the effect of increasing ω_n in the step response. It can be seen that high value of ω_n results in reduced error with low settling time.

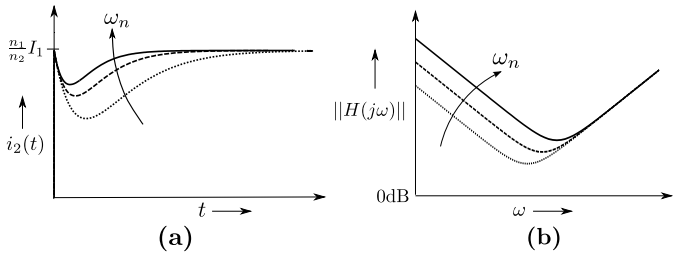

Fig. 4: Effect of variation in ω_n with $\zeta_1 = 1$ (a) step response of $i_2(t)$ (b) bode magnitude plot of $||H(j\omega)||$.

If K_p and K_i are selected such that

$$K_P K_m \gg \frac{R_L}{L_m}$$

we can approximate ζ_H in (16) as equal to ζ_n, i.e.

$$\zeta_H \simeq 1 \tag{25}$$

Bode magnitude plot of $||H(j\omega)||$ is shown in Fig. 4(b) for $\zeta_H = \zeta_n$ equal to 1. Increase in the value of ω_n increases the minimum value of $||H(j\omega)||$. This reduces the error in measurement of sinusoidal $i_1(t)$ throughout the frequency range of interest. ω_n is selected based on either the value of t_{min} or the maximum undershoot allowed using (23) or (24). The PI compensator parameters K_p and K_i are calculated using (17) and (20) with $\zeta_n = 1$. The system parameters L_m, R_L and K_m are expressed in (3) and (12).

IV. Experimental Results

A prototype current sensor, shown in Fig. 5, is built in the laboratory to verify the analytical results. An Indium Antimonide four-terminal SH-400 Hall element [6] is positioned in the air gap of toroidal tape-wound magnetic core made of Nickel-Iron alloy. The PI compensator is implemented using OpAmp (LM301) based feedback circuit along with a class-B power amplifier at output stage as shown in Fig. 6. The Hall element is biased with constant voltage, which keeps its output less dependent on temperature compared to constant current biasing [7].

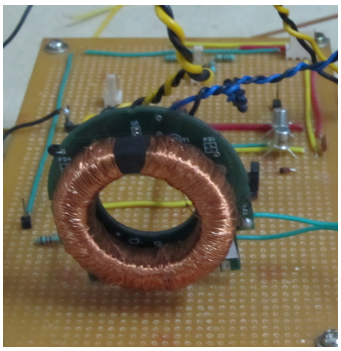

Fig. 5: Photograph of 300A Hall-effect current sensor built in laboratory to validate analytical results.

Specifications of the current sensor are given in Table I. Table II contains the values of system parameters calculated using Table I, (3) and (12).

TABLE I: Specifications of the current sensor built in laboratory.

n_1	n_2	l_g	A_c	K_h	r_2	R_B
1	2000	1.1 mm	59.4 mm^2	5.0 mV/mT	36Ω	100Ω

TABLE II: Calculated system parameters to design $G_c(s)$.

L_m	R_L	K_m
271.4 mH	136 Ω	42.1 s^{-1}

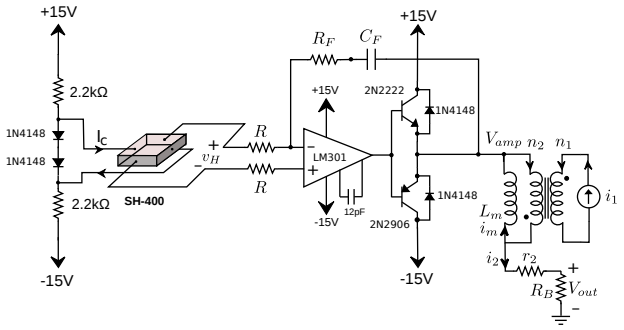

Fig. 6: Schematic of the current sensor with PI compensator using single operational amplifier.

A. Model Verification

A proportional-resonant current controlled single phase voltage source inverter with pure inductive load is built in laboratory to be used as current source to generate sinusoidal reference current and to validate steady state performance of the current sensor. An optimized Proportional-Resonant current controller is designed based on the procedure given in [5]. An IGBT based half bridge voltage source inverter with pure resistive load is used to observe step response.

Three different sets of K_p and K_i are selected to validate the model and to show the variation in performance with gains of the compensator. The results using simulation model and respective experimental results obtained with the current sensor are shown in Fig. 7. Though PI compensator ensures zero steady state error for DC, the settling time may become high with arbitrary values of the compensator gains. In Fig. 7 it can be observed that increasing the value of K_p reduces the initial undershoot, but the settling time is approximately 8 ms, which is not desired.

B. Design Example: PI Compensator

The approach to select the values of K_p and K_i that was outlined in Section-III, has been followed to design PI compensator for the current sensor set-up with parameters shown in Table I. Using the values in Table II and $\zeta_n = 1$, (20) can be expressed as:

$$\omega_n = 21.05K_p + 250.7 \tag{26}$$

As discussed in section III a large value of ω_n is desired for fast dynamic response. PI compensator is implemented using single operational amplifier as shown in Fig. 6. Ideally a very large value of K_p can be implemented assuming ideal behaviour of operational amplifier, but the non-idealities restricts K_p to a maximum limit. In this way ω_n can be selected based on very large value of K_p in (26).

1) Realization of $G_c(s)$ with single operational amplifier: The Hall element produces output voltage at its two terminals with common mode and differential mode components [7]. The differential component is proportional to magnetic field, which needs to be passed through the compensator $G_c(s)$. Realization of $G_c(s)$ with single operational amplifier limits the maximum gain attained along with high common mode

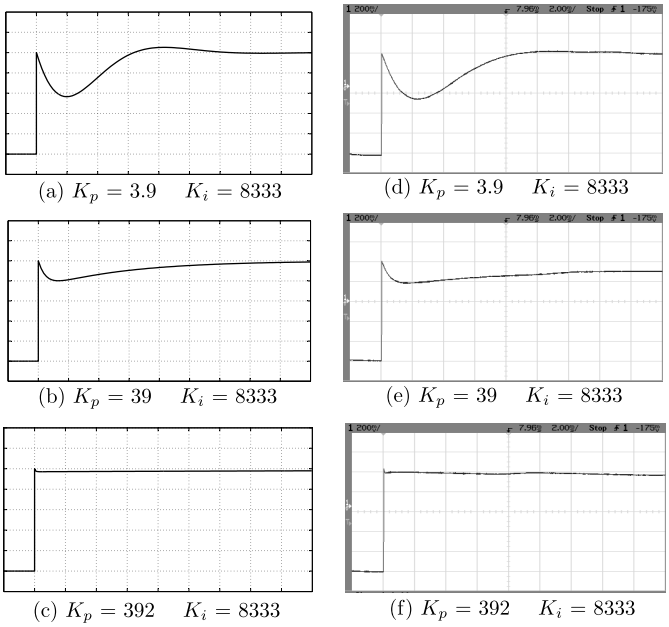

(a) $K_p = 3.9$ $K_i = 8333$ (d) $K_p = 3.9$ $K_i = 8333$

(b) $K_p = 39$ $K_i = 8333$ (e) $K_p = 39$ $K_i = 8333$

(c) $K_p = 392$ $K_i = 8333$ (f) $K_p = 392$ $K_i = 8333$

Fig. 7: Comparison of simulation and experimental results for a step input current and different values of K_p.
(a)-(c): $V_{out}(t)$ from the simulation model, (d)-(f): $V_{out}(t)$ from the experimental hardware.
vertical scale: 4A/div, time scale: 2ms/div.

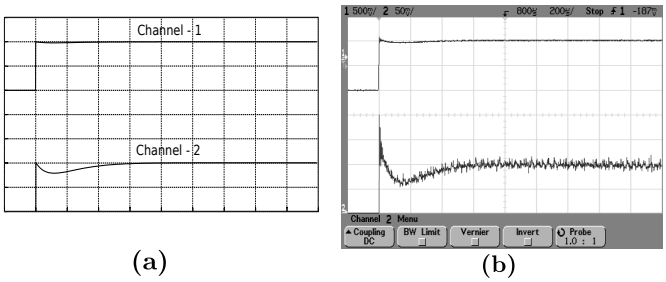

(a) (b)

Fig. 8: Comparison of simulation and experimental $V_{out}(t)$ waveforms for large ω_n with a 20A step primary current. Ch-2 displays Ch-1 with 10x magnified vertical scale about the steady state value (a) response of the simulation model (b) experimental result.
K_p = 392, K_i = 1714134.
Ch-1: 500mV/div, Ch-2: 50mV/div, time scale: 200μs/div.

rejection ratio required. K_p = 392 is selected considering these limitations in the circuit shown in Fig. 6. Various parameters are calculated based on this K_p and listed in Table III.

TABLE III: Parameters of PI compensator realized with single operational amplifier.

K_p	K_i	R	R_F	C_F
392	1714134	1.2 kΩ	470 kΩ	486 pF
ζ_n	ω_n	t_{min}	$I_{2_{min}}$	
1.0	8495	117.7 μs	97.8%	

A step rise of 20A in primary coil should be measured as V_{out} = 1.0V across 100Ω burden resistor. Fig. 8(a) and Fig. 8(b) show simulation and experimental result of step

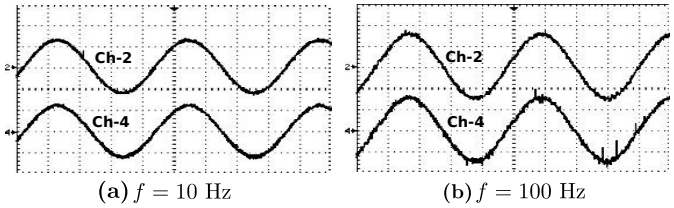

(a) $f = 10$ Hz (b) $f = 100$ Hz

Fig. 9: Experimental results: low frequency sinusoidal current measurement with the laboratory current sensor using single OpAmp PI compensator: K_p = 392, K_i = 1714134.
Ch-2 (5A/div): reference current, Ch-4 (5A/div): current sensor output. time scale:(a) 25ms/div, (b) 2.5ms/div.

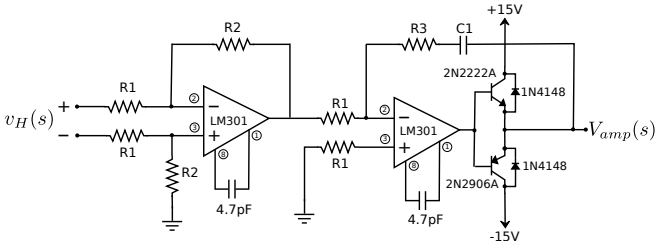

Fig. 10: Circuit realization of PI compensator, $G_c(s)$ using two operational amplifiers with class-B power amplifier at output stage.

response of the prototype current sensor with the designed PI compensator. Selection of large value of K_i in this case increases ω_n, which in turn reduces settling time. An undershoot of 3.35% at 150μs is observed in the experiment, which is superior to that from Fig. 7. The deviations from simulation results listed in Table III are due to tolerance in circuit components and the assumptions of the current sensor analysis stated in Section-II.

Experimental waveforms for 10Hz and 100Hz sinusoidal current excitations are shown in Fig. 9. This indicates that a single OpAmp compensator is sufficient from a low frequency perspective.

2) Realization of $G_c(s)$ with two operational amplifiers: Very high value of K_p and K_i can be attained, if PI compensator is realized as shown in Fig. 10. External single pole compensation is required to extract high gain bandwidth product as well as high common mode rejection ratio. The limited rise time (35ns) and fall time (300ns) of the transistors used in the current buffer stage along with the finite slew rate of the operational amplifiers (10V/μs) limit the $\frac{\mathrm{d}i}{\mathrm{d}t}$ tracking of the current sensor.

Expression of $G_c(s)$ in Fig. 10 is given by:

$$G_c(s) = \frac{R_2}{R_1}\left(\frac{R_3}{R_1} + \frac{1}{R_1 C_1 s}\right) \tag{27}$$

Compensator parameters are listed in Table IV with new value of K_p and respective components value corresponding to the schematic in Fig. 10.

Fig. 11 shows the experimental waveforms obtained using two OpAmp high gain compensator. The lower waveform is magnified view of the step response shown in channel-1 of the figure. Minimal undershoot is observed in this case as the

TABLE IV: Parameters of PI compensator realized with two operational amplifiers.

K_p	K_i	$R1$	$R2$	$R3$	$C1$
15510	2.54x10^9	1.0 kΩ	470 kΩ	33 kΩ	185 pF
ζ_n	ω_n	t_{min}	$I_{2_{min}}$		
1.0	326736	3.1 μs	99.94%		

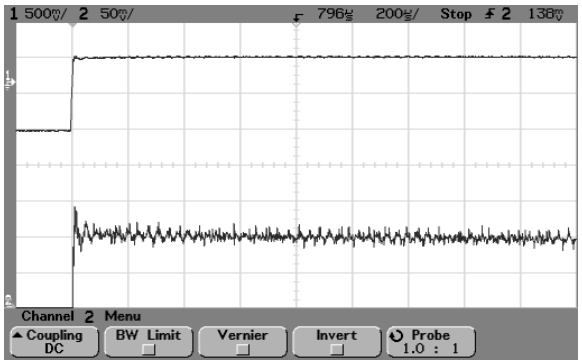

Fig. 11: Experimental waveform of $V_{out}(t)$, when PI compensator is realized with two operational amplifiers for a 20A step primary current. Ch-2 displays Ch-1 with 10x magnified vertical scale about the steady state value. $K_p = 15510$, $K_i = 2.54\text{x}10^9$.
Ch-1: 500mV/div, Ch-2: 50mV/div, time scale: 200μs/div.

settling time is $\sim$ 3 μs. The spike at the step jump is due to parasitic elements, which can be reduced with improved winding of compensating coil and better packaging and layout of circuit components.

Frequency response of the laboratory current sensor is measured with analog network analyzer [9]. The observed data is plotted in Fig. 12. The 3dB bandwidth is found to be 265 kHz for the current sensor. The initial glitch around 10Hz is observed due to lower frequency limitation (5Hz-15MHz) of the network analyzer. The step response of the laboratory current sensor is compared with the commercial current sensor [8], and observed to be similar during turn-on transient of IGBT into a resistive load as shown in Fig. 13. Both the sensors have $\frac{\mathrm{d}i}{\mathrm{d}t}$ limitations, which lead to a 10μs rise time in output compared to the applied step.

V. Conclusion

An equivalent circuit of closed loop compensated Hall-effect current sensor is derived based on practical assumptions. This is used to develop a model of the current sensor. Dynamic performance of the current sensor with PI compensator is analyzed. This results in zero steady state error for DC measurement. A tuning procedure based on analytical expression of the step response is derived for the PI compensator. A high value of ω_n ensures fast dynamic response as well as good steady state performance. A prototype current sensor is built in laboratory to verify the analysis. The experimental waveforms match closely with the results obtained using the simulation model. A PI compensator for the laboratory current sensor is designed using the procedure developed in this paper. The finite open loop gain of operational amplifier to realize the PI compensator limits the reduction in error in output of the sensor. This is overcome by using two cascaded operational amplifiers with very high gain-bandwidth product. The final design results in a current sensor with 265 kHz bandwidth, which is comparable to commercially available current sensors.

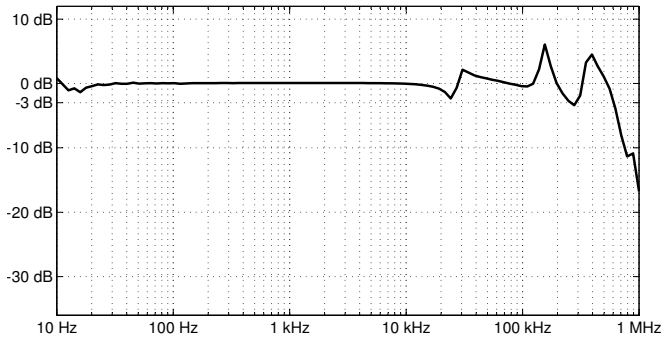

Fig. 12: Frequency response measurement of the laboratory current sensor. $||\frac{V_{out}(j\omega)}{i_1(j\omega)}||$ with gain normalized to one.

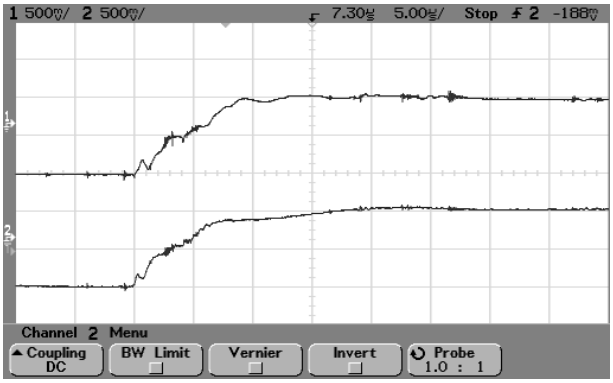

Fig. 13: Comparison of step response measurement. Ch-1: the laboratory current sensor, Ch-2: commercial current sensor [8].
Ch-1, Ch-2: 10A/div, time scale: 5μs/div.

References

[1] Bin Jin, *Modeling and implementation of a smart current sensor*, Proceedings of the 1992 International Conference on Industrial Electronics, Control, Instrumentation, and Automation, 1992. Power Electronics and Motion Control, vol. 3, pp. 1550-1555, 1992.

[2] Y. Suzuki, K. Yamasawa and A. Hirayabayashi, *Analysis of a Zero-Flux Type Current Sensor Using a Hall Element*, IEEE Translation Journal on Magnetics in Japan, vol. 1, pp. 165-170, 1994.

[3] P. Pejovic and D. Stankovic, *Transient analysis of compensated Hall-effect current transducers*, Proceedings of 21st International Conference on Microelectronics, 1997. , vol. 2, pp 569-572, 1997.

[4] J Pankau, D. Leggate, D.W. Schlegel, R.J. Kerkman and G.L. Skibiniski, *High-frequency modeling of current sensors [of IGBT VSI]*, IEEE Transactions on Industry Applications, vol. 35, pp 1374-1382, 1999.

[5] D. G. Holmes, T.A. Lipo, B.P. McGrath and W.Y. Kong, *Optimized Design of Stationary Frame Three Phase AC Current Regulators*, IEEE Transactions on Power Electronics, vol. 24, pp 2417-2426, 2009.

[6] Pacific Scientific-OECO, "SH Series Hall Sensors", *Available Online: www.hwbell.com*, 2013.

[7] Pavel Ripka, *Magnetic Sensors and Magnetometers*, Artech House, 2001.

[8] LEM, "LA 55-P Current Transducer", *Available Online: www.lem.com*, 2013.

[9] AP Instruments Inc., "AP 200 ISA Analog Network Analyzer", *Available Online: www.apinstruments.com*, 2003.